Impact Assessment of New Generation High Speed Agricultural Tractor Aerodynamics on Transportation Fuel Consumption and Related Phenomena

Eyub CANLI (ecanli@selcuk.edu.tr)
Selçuk Üniversitesi: Selcuk Universitesi https://orcid.org/0000-0002-9358-1603
Hanifi Kucuksariyildiz
Karamanoglu Mehmetbey University: Karamanoglu Mehmetbey Universitesi
Kazim Carman
Selçuk Üniversitesi: Selcuk Universitesi

Research Article

Keywords: Agricultural tractor, Aerodynamic resistance, CFD, Drag, Exhaust emissions, Fuel consumption

Posted Date: March 9th, 2022

DOI: https://doi.org/10.21203/rs.3.rs-1311879/v1

Abstract

New generation agricultural tractors contribute to transportation by increased travel speeds. There is not any available aerodynamic data on authentic agricultural tractor form. On-road transportation by tractors is between 8 to 30% of their operational time. In this work, two agricultural tractors are modelled via computational fluid dynamics for nine different speeds to determine aerodynamic resistances. Corresponding speeds are 10 to 80 km/h with 10 km/h increments and additionally 5 km/h. Reynolds number changes between 1.6×10^5 and 2.98×10^6. The characteristic lengths are taken as the square root of the streamwise projected area of the tractor geometries. Aerodynamic forces exerted on the tractors change between 3 N to 746 N. The calculated drag coefficients are found as independent from Reynolds number and are 0.6 and 0.78 for the two different types of driver compartments. Constant speed travel scenarios are analysed. The approximated aerodynamic related fuel consumptions for one-hour changes between 0.002 to 8.28 lt/s which correspond to 0.001 to 5.76 kg/s carbon emission. A potential improvement in decreasing aerodynamic resistance about 20% is discussed by spatial data. Since the conducted work is being regarded as the first instance in the literature, it is estimated that several consecutive reports will be triggered.

Introduction

Agricultural tractors are gaining new abilities. Their power, torque, speed, operator comfort offerings, utilities and features are ever increasing. Today, transportation by agricultural tractors with relatively high speeds is common. In a very recent work of Mattetti et al. (2021), 579 h of real-world operation from an agricultural tractor is processed and 8% of the operation is found to be on-road with travel speeds between 40-50 km/h. More interesting is, the engine power values approach to field operation values during on-road transportation. Harland et al. (2014) suggest that 30% of agricultural tractor included traffic incidents occur in urban areas. Authors also indicate that most frequent incidents among mentioned percentage are in 55 mph speed limit roads. They add that seasonal activities contribute to the intensity of incidents. Mederle et al. (2015) justifies the reason of agricultural tractor usage in road transportation and also state that agricultural tractor tires are used in on-road transportation at a rate of 30%. Therefore, they conducted an experimental tire examination for transportation speeds of 50 and 60 km/h travel speeds. Cavallo et al. (2015) focused on expectations of farmers regarding technological developments in agricultural tractors. One of the three major expectations is on increasing agricultural tractors for on-road transportation. Authors emphasize motivating parameters for high-speed agricultural tractors and also state that agricultural tractors are being used in on-road transportation. Finally, a domestic study determined that 50% of operational time of agricultural tractors are dedicated to on-road transportation (Altintas 2015). However, the impact of on-road transportation on energy consumption and environment has not been addressed. Its aerodynamic component seems to be missing totally. One of the important aspects of aforementioned transportation by agricultural tractors is aerodynamic performances of high-speed agricultural tractors. Aside statistics related to usage of agricultural tractors in transportation, it is now understood that there is almost no work giving aerodynamic performances of

agricultural tractor form. Even if the necessary statistics are obtained for the usage, aerodynamic aspect is still absent, and it is needed to be addressed for breaking total impact into sources. Main field of application of agricultural tractors are off-road agricultural fields and therefore aerodynamic investigation has not been done by the scientific and engineering communities. However, their transportation contribution should not be underestimated in the present day. Especially 60 to 80 km/h speeds are now feasible. As a general rule of thumb, 40 km/h is regarded as a threshold for aerodynamic resistance. However, this threshold is generated for vehicles having drag coefficient (C_D) about 0.2 or 0.3. If C_D about 0.5 is considered, the limit reduces to 30 km/h. Adding increased surface areas of high C_D vehicles, aerodynamic investigation of agricultural tractors deserves attention as commercial tractors do.

As mentioned earlier, after spending months on literature by several databases, it is concluded that there is not any single aerodynamic work published on aerodynamics of agricultural tractors. Only two papers, dealing with a type of meshing technique in Computational Fluid Dynamics (CFD) used tractor geometry since this geometry has the needed complexity by the authors to test their meshing technique (Hsu et al. 2016, Xu et al. 2016). However, the two papers do not deal with physics of the phenomena or examine the case. Instead, they focus on the effect of the mesh types. Only provided information related to the present work is the C_D of the tractor model, i.e., about 0.8 for 11 m/s inlet velocity and Re about 4.5×10^6. As it will be shown in the present work, drag coefficients are not consistent with the above mentioned two papers. However, drag coefficient definition based on characteristic length and drag components can cause differences between results. Unfortunately, authors did not report the force values. On the other hand, wake structures downstream of the tractors have qualitative resemblances, which are also mentioned in the results section for comparison. Other than that, as explained, there is no work in the literature focusing on aerodynamics of agricultural tractors.

Aerodynamic investigations on commercial vehicles can give an idea for a framework of aerodynamic investigations on agricultural tractors. Commercial vehicles and commercial tractors, trucks in other words, have high drag coefficients and high form and friction drag surfaces as agricultural tractors do. Therefore, not only their CFD framework is useful for the current case but also some aerodynamic aspects and results can be used for the current case. It is clear that numerous passive flow control devices are adapted by commercial tractors for improving fuel economy and reducing negative impacts. Khosravi et al. (2015) used CFD in order to investigate effects of several append devices as passive flow controllers on drag coefficients of commercial tractor trailer couples. They managed to obtain 41% reduction in drag coefficient by means of a combination of the append devices. Kim et al. (2017) used wind tunnel and Particle Image Velocimetry (PIV) in order to investigate cab-roof fairings as an aerodynamic modification for commercial tractor trailer combinations experimentally. Authors also used CFD in their investigation. Several geometric modifications on the cab-roof fairings are taken as geometrical parameters by the authors. Fore body is emphasized as being a major contributor to aerodynamic drag. 19% drag reduction is obtained by the fairings. A similar work is reported by Malviya et al. (2009). Authors used experimentation and CFD together. Drag contributions of several parts of commercial tractor trailer combination are given. Passive flow control geometries alongside an active

flow control device named as “moving surface boundary layer control” cylinder, are examined. Authors claim that the active flow control device can decrease fuel consumption up to 13%. Hariram et al. (2019) report an extensive review on aerodynamics of commercial truck and trailer combinations. Three main conclusions of the authors support present work. They are; importance of fore body geometry that discriminate USA trucks from Europe trucks; different contributions of CFD, wind tunnel testing and truck testing; drag reduction potential up to 10%. Kim et al. (2019) used wind tunnel and PIV in order to provide quantitative spatial resolution of flow around commercial tractor-trailer combination with several passive flow control geometries. 26% drag reduction is determined by the authors. Mosiężny et al. (2020) use Reynolds Averaged Navier Stokes (RANS) turbulence modelling for steady solution and Delayed Detached Eddy Simulation (DDES) for transient CFD solution of commercial tractor-trailer combination. Authors tried an active flow control arrangement at the rear part of the investigated vehicle and obtained 11% drag reduction. The CFD approach of the work is also worth to be mentioned. Aerodynamics of a vehicle or truck type is also important for platooning, which is highly studied in transportation. The work of Dávila andNombela (2011) can be given as an example. Authors report 20% drag reduction for some of the vehicles in the platoon, mostly due to the aerodynamic features of the leading vehicle. Almost all reviewed literature works emphasize aerodynamic resistance impact on fuel consumption and related negative impacts on environment due to exhaust emissions. Additionally, it is understood that passive flow controllers are widely studied and also commercially available. The current experience on aerodynamics of commercial tractors justifies a work on aerodynamics for transportation by agricultural tractors. This experience is also an advantage that can be adapted rapidly and hence give positive results in relatively short times.

Drag force acting on ground vehicles have several components emerging from different sources. Breaking down drag force into components creating a chance to reduce them by focusing on a certain source. Real vehicle models can be used for this task as well as simplified models that isolate most of other sources. There are instances for both approaches. Wiedemann (1996) stresses importance of wheel turning and ground moving in wind tunnel tests. Author shows that three important factors are not available in conventional wind tunnel tests, i.e., ground relative motion, rotation of the wheels and air flow through engine cooling system. It is also mentioned that 1% drag reduction corresponds to about 10 to 15 kg weight reduction. Sivaraj et al. (2018) study a base-bleed solution for drag reduction on a simplified model geometry. The simplified car model is modified with a base-bleed geometry in wind tunnel tests and 6% drag reduction is attained. Vignesh et al. (2019) focus on front and read windscreens and hood angles by using CFD. Authors determine the best arrangement of angles for the lowest drag value. Their car model is also a simplified one, imposes almost only the three geometrical parameters. This simplified geometry approach actually based on pioneering works in 70s and 80s (Ahmed et al. 1984, Morel 1978, Templin &Raimondo 1986). Whether it is due to petrol crisis or not, starting from 70s, drag reduction is a main concern and dealing with it has been done mostly by simplified models that isolate most of the factors and focus on one or two main parameters. Le Good andGarry (2004) lists about 25 reference simplified models. However, it is again evident that there is not any reference geometry that features characteristics of agricultural tractor form. Therefore, it is suggested by the authors of the present work

that breakdown of drag relating to the agricultural tractor geometry should be done in the future and reference geometries can be developed in order to investigate drag components.

Before proceeding further, it should be noted that there are works on tractor transportation (Jokiniemi et al. 2016) but they are related to mechanical resistances. Gao et al. (2019) view eco-driving potentials for diesel vehicles and drag reduction significantly takes place in the list. However, the test cycle that is cited by the authors are for light duty diesel vehicles and it is not clear that transportation by agricultural tractors is subjected to any regulation at all. The aerodynamics of agricultural tractor will also provide for additional aspects such as air conditioning in the tractor cabin since previous works is done for stationary or quasi-stationary conditions (Oh et al. 2020).

Transportation by agricultural tractors with high travel speeds is expected to have high impact on energy utilization and environmental effects. However, it is not possible to make an assessment without aerodynamic performance perspective. In the current state of the literature, no relevant aerodynamic assessment has been encountered in the literature. Previous studies on agricultural tractor energy consumption focus on tire inflations and other issues considering off-road operations related with traction (Janulevičius &Damanauskas 2015). However, it is apparent that present day capabilities of agricultural tractors, including travel speeds, enable them for high-speed transportation. There are also literature papers, that have already been mentioned, dealing with the on-road transportation with agricultural tractors (Altintas 2015, Cavallo et al. 2015, Harland et al. 2014, Mattetti et al. 2021, Mederle et al. 2015). Nevertheless, it is known that there are numerous works for other vehicles. Xie et al. consider aerodynamic drag for arranging distances between vehicles in platoons, especially commercial tractors or trucks (Xie et al. 2020). It is seen that drag coefficient changes about 50% according to the distance between platooning vehicles. Authors emphasized its energy implications. Drag is very related for energy consumption and environmental impacts and hence, researchers are trying to find innovative geometries to reduce drag by having inspirations from nature (Huang et al. 2021). Obtained experiences are adapted in real world applications. The necessity of drag data for a vehicle form can be assessed by life cycle assessments (Schäfer et al. 2006). Authors consider drag coefficients originating from vehicle bodies and tires during constructing their models. It is also visible that vehicles they used have drag coefficient between 0.2 and 0.3, that are quite small considering agricultural tractors. Similar vehicle modelling works considering aerodynamic drag for a type of vehicle in respect of energy issues exists in the literature (Tian et al. 2019).

In this work, two new commercial agricultural tractor models, originally emerging from a single model, are adapted for CFD investigation. On road high speeds scenarios that may be due to transportation are used for investigating flow around the tractor. Aerodynamic drag forces acting on the geometry are determined. Fuel consumption and related carbon emission are approximated. Experience related to the CFD modelling is shared since this work is one of the two examples in the literature. A framework for future studies is presented for reducing drag force during transportation operations by agricultural tractors. It is projected that scientific community will respond rapidly and diversify findings to give a complete resolution on the topic.

Method

The 3D solid models for agricultural tractors that can do the transportation tasks on road with relatively high speeds were obtained from Erkunt Traktör Sanayii A.Ş, an agricultural tractor manufacturer in Turkey. The model number is “Nimet 75”. The main difference between the two models is based on driver compartment. One model is isolated from ambient by a “cabin” and the other one has direct contact with the ambient. However, commercial models are too complex for CFD modelling. Therefore, surfaces are simplified by deleting some details. By doing so, the geometries are adapted for CFD. The final models are shown in Figure 1. Some dimensions are given in Figure 2.

Before meshing of the calculation domain, flow field is constructed with two main zones. The first zone is the zone that surrounds the tractor at proximity. This zone is called internal enclosure. The second zone surrounds the internal enclosure and called external enclosure. Together with the tractor geometry, three solid volumes exist. However, for CFD purposes, only fluid volumes around the solid surfaces are enough since the surfaces can act as fluid-solid interfaces by manual selection. Therefore, meshing cost of the solid parts is avoided by erasing them. Solid domains are only for creating enclosures. Using solid domains in the preparing of the calculation domain, i.e., fluid volumes and interface surfaces between solid and fluid volumes provide ease. Constructing fluid values without solid model would be too hard, complex, and costly. The CFD investigation in this work is a steady analysis. Therefore, flow around the tractor is symmetrical according to middle plane of the tractor in movement axis. Accordingly, only half of the enclosure volumes are transferred into meshing software. Figure 3 shows the 3D volume that contains one side of the symmetrical parts of the two enclosures. This figure also marks dimensions of the enclosures. As a general practice, preliminary CFD runs were performed and accordingly boundaries are placed distant enough in order to reduce their effect on the solution. Actually, this is done since known values are used in boundary conditions and those boundaries sufficiently distant from the tractor ensures that the boundary conditions are valid. Especially, outlet boundary has the most distant location due to the spatial length necessity of the wake flow of the tractor model to be diminish at the outlet. All domain sides except the road and the tractor surfaces (no slip walls) are set to symmetry boundary condition. Inlet is arranged as having one directional velocity inlet with 5% turbulence intensity. The intensity value is about 1% in controlled wind tunnel tests (Ahmed et al. 1984). In reality, it can be higher by atmospheric conditions. Turbulence intensity of 5% is regarded as a steady real world air condition. Also, CFD method approaches to necessary level right after the inlet during iterations (Canli et al.). Turbulence intensity at the inlet is just for estimating values necessary for conducting numerical iterations. Tractor model surfaces and road are modelled as no slip walls. One may question boundary conditions on tractor surfaces and the road since some of the tractor surfaces are porous, some are rotating in reality. Also, relative motion between the tractor and the road is generally simulated by means of moving wall in CFD. However, though those boundary conditions would affect aerodynamic performance of the agricultural tractors, present work is the first step towards the ultimate accurate results. The main trend and approximate results reported in this work will further approach to reality and accuracy by means of further studies that will focus different parameters. The assumptions and simplifications in this work isolate parameters that are examined in the present work and enable an easier comparison.

Meshing fluid volumes for a successful CFD analysis is essential. However, tractor geometry, even with its simplified form, is very complex for a structured mesh. Inflation layers cannot be generated by the software. Therefore, internal enclosure is meshed with finer element sizes and external enclosure is meshed with coarser elements. Element types are tetrahedral unstructured elements. By doing so, 2 layers of mesh elements sizes are obtained. Internal enclosure has constant element size. External enclosure grows to maximum elements size starting from the internal enclosure element sizes. Three meshes were constructed for mesh independency. They are labelled as coarse, medium, and fine. Internal mesh element size doubled for each mesh transitions, i.e., coarse to medium and medium to fine. For nodes, linear distribution is dropped, and program controlled quadratic interpolation is used for increased number of nodes considering effectiveness of the CFD code. Therefore, all node numbers are higher than the element numbers.

Turbulence model benchmarking were done with two different Reynolds Averaged Navier Stokes (RANS) turbulence models. Selected turbulence models are k-ω SST and Realizable k-ε turbulence model with standard wall functions. k-ω SST turbulence model is the default turbulence model that Ansys Fluent version 20 proposes. This turbulence model uses k-ω in the wall proximity and transits to k-ε far from wall. Therefore, mesh resolution near tractor walls requires dimensionless wall distance y^+ to be below 1. However, due to the complex geometry of the solid model, it is not possible to meet this criterion with the best level of confidence. Therefore, Realizable k-ε turbulence model with standard wall functions was also tried since standard wall function work between $y^+ \approx 11$ and 500. Tractor geometry is too complex to have a structured mesh having inflation layers on solid boundaries. The scale of edge sizes on the geometry varies greatly. Accordingly, an unstructured mesh having smallest possible elements were aimed. On the other hand, standard wall functions tolerating the high y^+ values enable the simulation. The default turbulence model k-ω SST is then provides a comparison tool where no wall functions were utilized with relatively high y^+ values. The difference between the two model solely arises from the proximity of the wall and boundary layer dealing method. The comparison, which is also used for mesh structure evaluation, gives the effect of wall functions.

In order to examine mesh convergence or independency, three different unstructured meshes were tried, namely, coarse, medium, and fine. Table 1 presents element numbers and node numbers of the three meshes. Mesh quality statistics are given in Table 2.

Table 1
Element and node numbers of the three meshes for mesh independency

		Cabin Version		Platform Version	
Mesh ID	**Element Size in Internal Enclosure (mm)**	**Element Number**	**Node Number**	**Element Number**	**Node Number**
Coarse	160	176,491	243,580	300,351	413,739
Medium	80	1,018,689	1,382,640	1,157,975	1,573,442
Fine	40	6,864,950	9,243,257	7,086,998	9,544,426

Table 2
Mesh statistics

Mesh Statistics		**Cabin Version**			**Platform Version**		
Element Quality		**Coarse**	**Medium**	**Fine**	**Coarse**	**Medium**	**Fine**
	Min.	0.01	0.05	0.12	0.02	0.02	0.05
	Max.	0.99	0.99	1	0.99	0.99	1
	Ave.	0.83	0.84	0.85	0.83	0.84	0.85
	Std. Dev.	0.1	0.1	0.1	0.1	0.1	0.1
Skewness	**Min.**	0	0	0	0	0	0
	Max.	0.99	0.99	1	0.99	0.99	0.99
	Ave.	0.22	0.21	0.2	0.22	0.21	0.2
	Std. Dev.	0.13	0.1	0.1	0.13	0.1	0.1
Orthogonal Quality	**Min.**	0	0	0.01	0	0	0
	Max.	0.99	0.99	0.99	0.99	0.99	0.99
	Ave.	0.76	0.78	0.79	0.77	0.78	0.79
	Std. Dev.	0.12	0.11	0.11	0.13	0.11	0.11

The difference between element numbers and node numbers for cabin and platform versions of the tractor models is due to the fact that fluid fills driver compartment while cabin leads to a void in that region. Also, a special measure was taken for the steering wheel during the meshing of platform version since steering wheel has a very small volume, resulting mesh element merging. A sphere of influence function surrounded steering wheel and kept the element size at 40 mm at that small volume. Considering only Table 1 and 2, based on self-experiences, medium and fine meshes seem adequate. Mesh instances are given in Figure 4 for cabin version. The internal enclosure mesh elements cover a big portion of the wake flow of the tractor models.

In order to evaluate results depending on mesh structure, drag coefficient (C_D) and aerodynamic drag force (F_D) acting on the tractor models were calculated. Drag force acting on the tractor surface is calculated by the Fluent software considering streamwise projected areas of mesh elements and then using integration. Normal pressure acting on a mesh surface coinciding tractor surface is multiplied with surface area, yielding the force and its streamwise component is calculated for summing them covering all tractor surfaces. After summing all forces on a specific direction, which is the streamwise direction in the present case, total force is calculated. However, mesh structure changes streamwise projected area of the tractors slightly. Nevertheless, this phenomenon is compensated by the calculation definition of C_D. Drag coefficient is calculated by below equation (1).

$$C_D = \frac{F_D}{\frac{1}{2} A \rho V^2} \quad (1)$$

In equation (1), F is the drag force, A is the streamwise projected area on the tractor, V is the inlet velocity and ρ is the air density at room temperature. Although viscous and pressure components of the drag force exist, their total is used in this study. Streamwise projected area values for whole tractor bodies are given in Table 3. The projected area values were calculated using Fluent by decreasing the minimum feature size value till the change in the projected area is below 0.1%. Actually, projected areas in Fluent are half of the values in Table 3 due to the symmetry boundary condition.

Table 3
Streamwise projected area values of the whole-body tractor models according to the three meshes

Mesh ID	Cabin Version	Platform Version
Coarse	4.088 m^2	3.104 m^2
Medium	4.096 m^2	3.124 m^2
Fine	4.104 m^2	3.138 m^2

Figure 5 presents changes in drag coefficient (C_D) and aerodynamic drag force (F_D) acting on the tractor models according to the mesh types for 40 km/h forward travel speed. Increasing element number by decreasing internal enclosure element size changes C_D and F_D acting on tractor models. However, cabin version and platform version respond differently. C_D and F_D decrease as mesh gets finer for cabin version. Nevertheless, k-ω SST turbulence model shows an asymptotic behaviour for cabin version. However, the change rate gets smaller as element number increases. On the other hand, making mesh finer for platform version marks a minimum and then increase the results for C_D and F_D. Also, medium and fine meshes for platform version gives close results. Before proceeding further, Table 4 is given for percentage changes of C_D and F_D according to mesh transitions. The F_D in calculation of C_D can be used as directly taken from Fluent but one must be careful about the area since half of the Table 3 values should be used.

Table 4
Percentage changes according to mesh independency for 40 km/h travel speed

	k-ε				***k-ω***			
	Cabin		Platform		Cabin		Platform	
	C_D	F_D	C_D	F_D	C_D	F_D	C_D	F_D
Coarse to Medium	8.3	8.1	6.5	5.8	8.3	8.1	7.3	6.7
Medium to Fine	4.0	3.8	2.3	2.7	2.1	1.9	2.8	3.2

Boundary layer evaluation in respect of mesh structure is also done according to y^+ values. Figure 6 and 7 show the comparison of y^+ values by means of surface contours, x-y plots and histogram plots, respectively for cabin and platform versions. Two dimensional “x-y” plot named visuals contain all y^+ values from all wall meshes. Contour and histogram visuals were plotted for the y^+ interval between 0-1000. Figures are for 40 km/h travel speed.

After evaluating all mesh dependent results together, fine mesh setup for the two-tractor model were found adequate in order to conduct further analyses. Standard wall functions can handle y^+ values below 500 by means of the fine mesh setups. Also, as shown by the histograms, most of the y^+ values are below 300. The change between medium and fine meshes are about 2% for C_D and F_D while platform version exhibits a minimum point at medium mesh. The qualitative extrapolation of the trends according to mesh comparison results imply that the rate of change also decreases. As a result, fine mesh setup was used in further analyses. Also, mesh metrics such as skewness, aspect ratio and orthogonal quality of the mesh elements would degrade greatly with smaller internal enclosure mesh element sizes. This would create undesired numerical error. On the other hand, using a personal computer, CFD calculation with coarse mesh results approximately in 20 minutes. Medium mesh and fine mesh CFD calculation times are 1 hour and 7 hours respectively. Total computation time is then approximately 70 hours. Postprocessing and evaluation extend the work period to 100 hours. Increasing mesh element number further would lead to unfeasible calculation times. One major problem with the complex tractor geometry, as stated by the literature (Hsu et al. 2016, Xu et al. 2016), meshing is a very hard task. Therefore, a dedicated future work on new meshing strategies is necessary.

One may wonder the effect of y^+ on the results. This can be answered by using two different strategies in CFD solution, i.e., using and not using standard wall functions. Since *k-ω* SST is the default turbulence model in the software and not using wall functions, a benchmarking was done between *k-ω* SST and Realizable *k-ε* with standard wall functions. Before turbulence model benchmarking results, numerical approach is explained in this part. Steady solution was used while gravity was ignored. Constant property air was selected as fluid, evaluated at room temperature. Inlet velocities for turbulence model benchmarking was selected as 11.12 m/s in normal direction to the inlet boundary. For further analyses, 1.388, 2.77, 5.55, 8.33, 11.11, 13.88, 16.66, 19.44 and 22.22 m/s inlet velocities were used additionally.

These velocities correspond to 5, 10, 20, 30, 40, 50, 60, 70 and 80 km/h traveling speeds. Reynolds number (Re) in this work was calculated by equation (2).

$$\mathrm{Re} = \frac{V \rho L}{\mu} \quad (2)$$

In equation (2), L is the characteristic length and was calculated by square root of the projected area. Dimensions of tractor geometry necessitates a hydraulic diameter like characteristic length. Therefore, square root of the projected area was used as the characteristic length value in Re calculation. In equation (2), μ is the dynamic viscosity of air. Air thermophysical properties were read from thermodynamic tables for 1 atm pressure and 20 ^{o}C temperature. The Re interval of the investigation is 186,291-2,982,270 for cabin version and 162,897-2,607,772 for platform version. Long commercial trucks/tractors and aerofoils use length while as the characteristic length while short obstacles use height, width, or hydraulic diameter for the characteristic length value. Agricultural tractor geometry resembles to a cube and therefore, characteristic length was calculated by taking square root of the streamwise projected area. Characteristic length L was calculated as 2.02 m for the cabin version and 1.77 m for the platform version. Accordingly, an updated version of Figure 3 is given as Figure 8 based on Characteristic length L.

Outlet boundary condition was set to pressure outlet at atmospheric gauge pressure. Spatial discretization scheme was selected as second order upwind scheme for all governing equations. Pressure velocity coupling was done according to Coupled scheme. High order term relaxation and pseudo transient options were enabled for a stable solution. This stabling effect slightly increases convergence time. General iteration cycle was limited with 500 iterations while C_D, mass flow balance and scaled residuals were monitored. It was observed that 300 iterations would be sufficient for C_D and mass flow rate balance converge to a fixed value. Scaled residuals of velocities and turbulence indicators were also below 10^{-8} value while scaled residuals of continuity approaches to 2×10^{-4}.

Turbulence model benchmarking between k-ω SST and k-ε is done by tractor model wakes and pressure iso surfaces at -10 Pa gauge vacuum values in Figure 9 and Figure 10 respectively. When the two figures are evaluated together, significant differences are hard to detect qualitatively. Viscous to total drag force percentages are 2.2 and 3% for k-ω SST and k-ε respectively, in case of cabin version. For platform version, the percentages are 2.6 and 3.6% for k-ω SST and k-ε, respectively. These results indicate that form drag is the main reason of the total drag. Also, the difference between the two approach is not significant. By the detailed mesh analyses and the benchmarking work, it was concluded that Realizable k-ε with standard wall functions is sufficient and accurate for the investigated case. The reason of selecting Realizable k-ε is also due to the fact that the turbulence model does not use a constant in calculating turbulent viscosity and instead, it calculates a coefficient by an additional equation. Also, it includes molecular viscosity in k and ε equations. The ε equation is also different from the standard model. This type of modification is recommended for separated flows and recirculation regions where form drag is important.

Power requirement due to drag force during transportation operation is approximately calculated by equation (3). In equation (3), P denotes power that is consumed to overcome aerodynamic drag force F_D. In order to calculate fuel amount, 0.2 total energy conversion efficiency is assumed in equations (4). In equation (4), $\dot{E}$ is the total energy conversion efficiency included energy consumption rate. By using lower heat value of the diesel fuel in equation (5), necessary fuel mass per second can be calculated.

$P = F_D V$ (3)

$$\dot{E} = \frac{P}{\eta} \quad (4)$$

$$\dot{m} = \frac{\dot{E}}{E} \quad (5)$$

Emitted amount of carbon is calculated by multiplying fuel mass with 0.849, which is the ratio of carbon mass in diesel fuel approximately.

Results And Discussion

Before presenting obtained results, one may wonder about the y^+ values for the minimum and maximum travel speeds. Figure 11 is given in order to show y^+ values for the minimum and maximum travel speeds similar to Figure 6 and 7.

Figure 11 shows that approximately 10% of the y^+ values are below 15 for the minimum travel speeds and 30% of the y^+ values are above 500 for the maximum travel speeds. In order to evaluate the effect of this distribution, the viscous drag is evaluated by its percentage in total drag using C_D viscous part percentage in total C_D, as given in Figure 12.

By viewing Figure 12 and comparing y^+ values of travel speeds with 40 km/h travel speed y^+ values, it is seen that overestimating due to lower speeds and underestimating due to higher speeds cause about 1% difference in viscous part of C_D. This is judged by the fact that Re independency is acquired in C_D according to the analysis results. Since the viscous drag in general has a very small contribution in general, about 4%, comparative evaluation of the results in the present work is regarded to be accurate. The Re independency is shown in Figure 13.

The Re interval of the investigation is 186,291-2,982,270 for cabin version and 162,897-2,607,772 for platform version. As shown in Figure 13, C_D is independent from Re in the investigation interval. Cabin version has about 0.6 C_D and the platform version has about 0.78 C_D. This phenomenon can be explained by the directly proportionality of F_D with travel speed and the definition of C_D which is expressed in equation (1). Since all other parameters in equation (1) are constant except the velocity and F_D, and the

proportionality between the two changing variables are not violated, C_D is not changing with Re. The proportionality between velocity and F_D is illustrated in Figure 14.

One major fact that should be considered in Figure 14 is that the drag force is calculated numerically. It is not an analytical value. CFD software uses static pressure values acting on tractor surfaces and integrates them for a specific direction. In the present case, the direction is the travel direction. The maintaining proportionality is the key phenomenon that should be examined. Travel speeds and accordingly Re increased 16 times from minimum speed to maximum speed and the proportionality between F_D and velocity is not changing. Before posing an explanation to the phenomenon, spatial data in three-dimensional space will be given in order to strengthen the physical comprehension. Another interesting result about F_D versus velocity is that F_D values are almost identical for the two tractor models. This suggests that cabin utilization has no major drawback in terms of aerodynamic resistance. Considering other comfort advantages of the cabin utilization, it is thought that cabin version is more logical in terms of aerodynamics.

The reason of aerodynamic resistance acting on the travelling tractor is mostly due to the form drag as previously indicated. Form drag is formed due to the pressure difference between upstream and downstream surfaces of the tractor. Flow impacts tractor surfaces and it attaches or detaches/separates to/from surfaces depending on the local boundary layer and pressure gradient. Dynamic pressure is converted to static pressure on the surfaces at different rates. Low-pressure wake occurs downstream of the tractor rear surfaces. Aerodynamic drag force acting on the tractor is a sum of static pressures on the tractor surface. Therefore, static pressure distributions are illustrated in Figure 15.

The static pressure distribution in Figure 15 is given in such a way that the contours have the same topology but indicated values are changing. This can be also done thanks to the same distribution trends between cases. It is seen that upstream front cover of the engine compartment is exposed to much of the high static pressure values for both tractor models. Therefore, it is evaluated that a porous structure in future works, considering the cooling systems and air suction of the engine will make some changes.

The static pressure distributions in Figure 15 for the cabin version are also show that front shield of the driver compartment (cabin) also exposed to high static pressure field. The platform model tractor has this pressure distribution on driver seat and inner surfaces of the driver compartment. Since low pressure surfaces at the downstream sides are very similar in terms of static pressure distribution, it can be concluded that the aerodynamic force action on the cabin front shield is almost equal to the aerodynamic force acting on driver compartment in the platform version. The driver comfort is then seriously reduced for the platform version as expected. The higher static pressure values on the cabin suggest a pitching moment acting on the tractor. In transient conditions, this pitching would result in vibration degrading driver comfort and induce health issues on long runs. According to above evaluations, it is seen that wind tunnel test are necessary for validation of the CFD approach. Another interesting result in Figure 15 is that front wheels and partially rear wheels are subjected to high static pressure fields. If wheel rotation will be included in future works, it is predicted that the resulting pressure fields and hence aerodynamic forces

due to the wheels will be higher. Maximum travel speeds lead to highest pressure levels up to 300 Pa above the gauge pressure. Also, below gauge pressure values are seen in the rear faces of the tractor models down to -200 Pa. The lowest pressure values are seen at side surfaces where flow accelerates due to fulfilment of mass conservation. Static pressure levels as low as -400 Pa are visible at side surfaces

From Figure 15, one may expect that the flow jet through the driver compartment at the platform version is somehow has high velocity values. Also, the wake of the tractor models can be wondered. Accordingly, velocity contours at the symmetry plane are shown in Figure 16. Velocity contour legends were prepared as between stagnant flow velocity, i.e., 0 m/s and two times the inlet velocity after rounding down the number. General wake topology for cabin version for different travel speeds are almost identical. This is also valid for the platform version. However, the wakes of the cabin version and platform version are not same. Nevertheless, the major portion of the low velocity wake is mostly downstream of the tractor lower half body. This implies that the driver compartment has minor effect on the wakes. Another thing to be stressed here is the possibility of different wakes for rotating wheels and moving road. These would affect the topology and size of the wake. Cabin version has a longer wake in downstream direction. In the absence of cabin wake, the wake of the platform version moves towards upwards. In the top of both tractor models, a slight velocity increase is apparent for lower travel speeds. The upstream of the front edge of the tractor models have a lower velocity region. Also, values of this region are seen in downstream of the tractors for a long narrow tape through the outlet at above the stagnant zone in the proximity of the road. One major interesting outcome is that the wakes are almost same sizes the tractors in a mirrored manner. These big wake regions have very low air movement in them. Also, the boundaries of the wakes create free shear layers with high momentum diffusivities. Wakes suggest a small clockwise vortex on the top region of the wake and a big counter-clockwise vortex on the bottom region of the wake for cabin version. In case of platform version, two similar magnitude vortexes at top and bottom regions of the wake are possible, resembling to Kelvin-Helmholtz instability.

The investigated range of Re number is known with intrinsic turbulence. However, by the solid boundaries of the tractors and interacting flow, geometry induced turbulence is also expected. Flow impact, separation, reattachment, recirculation, shear layers and possible vortex formations create turbulence. One way of examining turbulence magnitudes is to look for turbulent kinetic energy values. This is done in Figure 17 with again spatial data on the symmetry planes.

Figure 17 marks two major differences between tractor types. The first one is the location of turbulence peaks. The cabin version has its turbulent kinetic energy peak at above the cabin roof upstream edge. On the other hand, the turbulent kinetic energy peak values occur where the driver heat would exist in the platform version. One may expect this high turbulent flow would cause further noise and uncomforting conditions. The second major difference between tractor models is that the platform version creates more turbulence. This explains how a lower projected area value can give same amount of aerodynamic resistance force with the high projected area value. The surfaces in the driver compartment of the platform version poses an enhanced surface area for turbulence generation. This turbulence generation

draws flow energy and converts it into turbulence. The cost is the momentum diffusion to the driver compartment surfaces of the platform version. The air flow with increased turbulence levels tends to move towards the road surface for the cabin version. On the other hand, the increased turbulence level flow at platform version prevails longer and at about the height of the platform cap. This may lead to disadvantages when a trailer exists. Turbulent diffusion may affect the material that is transported in the trailer. Turbulence magnitudes downstream of the tractor for transportation purposes are actually open for further investigations and studies since vortex shedding, development, dissipation, turbulence diffusion and relevant phenomena strongly affect downstream of the tractor.

The downstream of the tractor models is also investigated in terms of pressure iso-surfaces, which mark vacuum regions according to gauge pressure in the downstream and proximity of the tractors. Results are given in Figure 18. Both tractor models do not generate significant vacuum regions around the surfaces and in the wake for travel speeds up to 20 km/h. At 20 km/h travel speeds, the cabin version generates 10 Pa vacuum around side surfaces and wheel proximities. This value should be different for rotating wheels. Also, a region of vacuum is generated above the cabin mostly at above the leading edge of the cabin cap. This is thought to be due to flow separation. Therefore, it is detected that flow separation starts to occur at 20 km/h. On the other hand, the platform version creates same amount of vacuum mostly in the wake. The cap of the driver compartment does not have comparatively significant vacuum region, probably due to the slower flow rates above the cap since below the cap is also open for flow and therefore same acceleration of cabin version is not seen here. The vacuum field in the wake of the platform version compensating the deficit above the cap, is due to the same amount of aerodynamic resistance forces acting on tractor models. This also explains the upward tending wake flow of the platform version. This conclusion is justified by remaining travel speed data. The vacuum fields of the cabin version enclose the cabin mostly. They have a half ring like shape. However, vacuum fields of the platform version elongate and extend in downstream direction. Transferred energy from upstream to downstream by the jet through driver compartment in the platform version prolongs iso-surface downstream of the platform version. This again is regarded as a drawback for trailer scenarios. On the other hand, moving road surface, rotating wheels, tractor surface porosity and different means of ventilation would effect vacuum fields of both models. It is also apparent that tractor wheels create and contribute the wake. Increasing travel speeds merges front wheel wakes with the general wake. It is seen that the choice of cabin or platform versions affects upstream iso-surfaces. Side volume of the cabin version iso-surfaces are bigger.

The spatial data emphasizes and explains aerodynamic forces acting on both tractor models for different travel speeds. However, the aerodynamic forces are also affecting the energy consumption of the tractors for transportation purposes. A tractor travelling at constant speed consumes energy for several and constant resistance forces. In order to decompose the resistance components, this work presents the aerodynamic component of the resistances. Figure 19 shows the necessary power to overcome the aerodynamic resistance for different travel speeds. The necessary power to overcome the aerodynamic force increase exponentially with travel speed as expected. It is seen that it can reach to about 16 kW. For more moderate speeds, the necessary power is between 2 kW and 12 kW. The necessary power for

overcoming aerodynamic resistance increases eight times as travel speed grows two times between 40 km/h to 80 km/h. If a 20% decrease in aerodynamic resistance can be achieved by improving tractor aerodynamic performance, 0.4 kW to 3.2 kW decrease in power requirement can be realized. However, this power amount increases due to energy conversion efficiencies. If 0.2 total energy conversion efficiency value is assumed from combustion to wheels through power delivery equipment, the necessary power amount grows five times. Accordingly, Figure 20 shows the necessary fuel amount per unit time in order to compensate this elevated power amount.

Figure 20 gives similar trends with Figure 19 and the essential content is then the diesel fuel amounts per unit time depending on travel speeds in order to overcome the aerodynamic resistance force. This data can approximately be used with the statistical data of tractor usage in transportation in order to determine the aerodynamic related fuel consumption. Another approximate approach can be using carbon emission data in order to evaluate environmental impact of the transportation by tractors. The aerodynamic resistance related carbon emission from tractors in transportation duties is approximated in Figure 21.

Aerodynamic sourced fuel consumption and carbon emission changes between 5.7×10^{-7} to 2.3×10^{-3} lt/s and 4×10^{-7} to 1.6×10^{-3} kg/s respectively. One hour transportation with the tractors corresponds to 3.6 lt diesel fuel and 2.52 kg carbon emission at 60 km/h travel speed. These values are 1.44 lt and 0.72 kg for 40 km/h while 7.92 lt and 5.94 kg for 80 km/h. Since any improvement in the aerodynamic performance is directly proportional for decreasing these values, there is a significant potential for working in geometric components of the tractor models. Above numbers would be more prominent when they are multiplied with possible agricultural tractor numbers in transportation. On the other hand, these values will help decomposing impacts of the transportation by tractors on environment.

Agricultural tractor drag coefficients are determined about 0.6 and 0.78, contradicting the values found in literature about 0.8 for high travel speeds that can be encountered in transportation duties by agricultural tractors. Since aerodynamic drag force is not encountered in the literature, it cannot be compared.

According to this work, tractor wheels, front face of the engine compartment, top surface above driver compartment and side surfaces of driver compartment are possible areas and regions to study further. However, CFD is not enough by itself. Wind tunnel test should be done in order to assess and validate CFD results. By this way, CFD geometries of agricultural tractors, their mesh structures, numerical models, schemes can be evaluated and improved. Subsequently, moving wall, wheel spinning, transient analyses, vortex shedding frequencies and other aspects should be determined. Major findings should be studied further systematically by characteristic tractor geometries resembling to Ahmed Body. After drag breakdown is achieved by systematic and detailed studies, aerodynamic performance improvement measures, by mostly passive flow structures, should be adapted from the experience in commercial tractors or trucks and tried. Finally, full scale agricultural tractors should be tested for various transportation scenarios. In a parallel manner, statistical research related to utilization of agricultural

tractors in transportation is necessary in order to assess possible impacts. This research scheme, described in this paragraph, can be extended further to agricultural tractor trailer combinations.

According to the literature survey, agricultural tractor aerodynamic performance can be improved up to 20% easily by adapting the experience in commercial tractors. Agricultural tractor front wheels, that are used for steering, have significant patterns and characteristic features. Impact of these wheels to aerodynamic resistance can be mitigated by temporary cases during transportation. Tires used in agricultural tractors have important parameters affect traction (Ekinci et al. 2015, Taghavifar &Mardani 2014) and some of them such as tire type, pattern, inflation pressure, position in general geometry, can significantly change aerodynamic behaviour. Base bleed structures through engine compartment and driver compartment can reduce wake dimensions. Vortex generators and turbulators can be adapted on top and side surfaces of cabin in order to separate and reattach the flow for narrower wakes. Tractor rear surface edges can be modified, as in commercial tractors, for pressure recovery. It is anticipated that present work will trigger future works of researchers in the field for above mentioned scenarios.

Conclusion

In this work, agricultural tractors that can be used in on road transportation tasks are adapted to CFD investigation for determining aerodynamic forces acting on them. The obtained aerodynamic forces that are attributed to transportation velocities are used for approximating aerodynamic sourced fuel consumption and carbon emission. It is thought that 20% drag force reduction is possible with future investigations on passive flow control devices that are tried on commercial tractors to adapt them on agricultural tractors during transportation operations. However, wind tunnel tests, vehicle tests and improved CFD simulations are needed in order to breakdown drag components and handle them separately in the future. Some key findings in the present work are summarized below.

- Reynolds number independency is realized between 1.6×10^{5} and 2.98×10^{6}. Corresponding drag coefficients are 0.6 and 0.78 for cabin and platform versions, respectively.
- Aerodynamic force acting on agricultural tractor during transportation changes between 3 N to 746 N. This corresponds to 0.02 kW to 82.82 kW energy input to the system if total energy conversion efficiency is assumed as 0.2 considering combustion, power delivery and other auxiliary steps.
- Cabin version is recommended in respect of aerodynamics since no significant drawbacks is found.
- Aerodynamic sourced fuel consumption and carbon emission changes between 5.7×10^{-7} to 2.3×10^{-3} lt/s and 4×10^{-7} to 1.6×10^{-3} kg/s respectively. One hour transportation with the tractors corresponds to 3.6 lt diesel fuel and 2.52 kg carbon emission at 60 km/h travel speed. These values are 1.44 lt and 0.72 kg for 40 km/h while 7.92 lt and 5.94 kg for 80 km/h.
- Front and rear wheels pose a resistance to the air flow and should be considered in future work in order to determine their absolute effect by considering wheel spin. Also, measures should be designed accordingly.

- Moving road, engine compartment porosity, effects of different cooling speeds are other factors to be considered in future CFD work.
- Aerodynamic experience on commercial tractors should be adapted for agricultural tractor transportation operations.
- Drag breakdown should be necessary for deeper understanding on the topic. A characteristic geometry, representing characteristic aerodynamic features of the agricultural tractor is needed.
- Wind tunnel tests are necessary for CFD validation.
- Real world 1:1 on road test should be the final step of aerodynamic measures for high-speed travelling agricultural tractors.

Declarations

Acknowledgement

The model used in this work is provided by Erkunt Traktör Sanayii A.Ş, an agricultural tractor manufacturer in Turkey. Authors greatly appreciate their supports in current mission for addressing aerodynamic performance of agricultural tractors in transportation. The model is adapted for CFD purposes and therefore does not reflect commercial version. This investigation is part of a general work in the context of Ph.D. thesis of Hanifı Kucuksariyildiz.

Compliance with Ethical Standards

Ethical Approval – Not Applicable

Consent to Participate – Not Applicable

Consent to Publish – Not Applicable

Data, Material and/or Code availability

Availability of data and materials – Not Applicable

Funding

The authors declare that no funds, grants, or other support were received during the preparation of this manuscript.

All acknowledgements are provided under the title of “Acknowledgement”.

Competing Interests

The authors have no relevant financial or non-financial interests to disclose.

Author Contributions

First author – Eyub Canli: CFD analyses; Data curation; Visualization; Writing – original draft. Second author – Hanifi Kucuksariyildiz: Literature review, Resources; Software; Data acquisition. Third Author – Kazim Carman: Conceptualization; Supervision; Writing – review & editing

References

1. Ahmed SR, Ramm G, Faltin G (1984): Some salient features of the time-averaged ground vehicle wake. *SAE Trans.*, 473-503
2. Altintas N 2015: The economic analysis of use of tractor in farms in Eskisehir province, Ankara University, Ankara, Turkey
3. Canli E, Ali A, BİLİR Ş Developing Turbulent Flow in Pipes and Analysis of Entrance Region. Acad. Platf. J. of Eng. and Sci. 9, 332-353 https://doi.org/10.21541/apjes.818717
4. Cavallo E, Ferrari E, Coccia M (2015): Likely technological trajectories in agricultural tractors by analysing innovative attitudes of farmers. Int. J. of Technol., Policy and Manag. 15, 158-177
5. Dávila A, Nombela M 2011: Sartre-safe road trains for the environment reducing fuel consumption through lower aerodynamic drag coefficient. 0148-7191, SAE Tech. Pap. https://doi.org/10.4271/2011-36-0060
6. Ekinci Ş, Çarman K, Kahramanlı H (2015): Investigation and modeling of the tractive performance of radial tires using off-road vehicles. Energy 93, 1953-1963 https://doi.org/10.1016/j.energy.2015.10.070
7. Gao J, Chen H, Li Y, Chen J, Zhang Y, Dave K, Huang Y (2019): Fuel consumption and exhaust emissions of diesel vehicles in worldwide harmonized light vehicles test cycles and their sensitivities to eco-driving factors. Energy Convers. and Manag. 196, 605-613 https://doi.org/10.1016/j.enconman.2019.06.038
8. Hariram A, Koch T, Mårdberg B, Kyncl J (2019): A Study in Options to Improve Aerodynamic Profile of Heavy-Duty Vehicles in Europe. Sustain. 11, 5519 https://doi.org/10.3390/su11195519
9. Harland KK, Greenan M, Ramirez M (2014): Not just a rural occurrence: differences in agricultural equipment crash characteristics by rural–urban crash site and proximity to town. Accid. Anal. & Prev. 70, 8-13 10.1016/j.aap.2014.02.013
10. Hsu M-C, Wang C, Xu F, Herrema AJ, Krishnamurthy A (2016): Direct immersogeometric fluid flow analysis using B-rep CAD models. Comput. Aided Geom. Des. 43, 143-158 https://doi.org/10.1016/j.cagd.2016.02.007
11. Huang S, Hu Y, Wang Y (2021): Research on aerodynamic performance of a novel dolphin head-shaped bionic airfoil. Energy 214, 118179 https://doi.org/10.1016/j.energy.2020.118179
12. Janulevičius A, Damanauskas V (2015): How to select air pressures in the tires of MFWD (mechanical front-wheel drive) tractor to minimize fuel consumption for the case of reasonable wheel slip. Energy 90, 691-700 https://doi.org/10.1016/j.energy.2015.07.099

13. Jokiniemi T, Suokannas A, Ahokas J (2016): Energy consumption in agriculture transportation operations. Eng. in Agric., Environ. and Food 9, 171-178 https://doi.org/10.1016/j.eaef.2015.11.001
14. Khosravi M, Mosaddeghi F, Oveisi M, Khodayari-b A (2015): Aerodynamic drag reduction of heavy vehicles using append devices by CFD analysis. J. of Cent. South Univ. 12, 4645-4652 https://doi.org/10.1007/s11771-015-3015-7
15. Kim JJ, Lee S, Kim M, You D, Lee SJ (2017): Salient drag reduction of a heavy vehicle using modified cab-roof fairings. J. of Wind Eng. and Ind. Aerodyn. 164, 138-151 https://doi.org/10.1016/j.jweia.2017.02.015
16. Kim JJ, Kim J, Hann T, Kim D, Roh HS, Lee SJ (2019): Considerable drag reduction and fuel saving of a tractor–trailer using additive aerodynamic devices. J. of Wind Eng. and Ind. Aerodyn. 191, 54-62 https://doi.org/10.1016/j.jweia.2019.05.017
17. Le Good GM, Garry KP (2004): On the use of reference models in automotive aerodynamics. SAE Tech. Pap. https://doi.org/10.4271/2004-01-1308
18. Malviya V, Mishra R, Fieldhouse J (2009): CFD investigation of a novel fuel-saving device for articulated tractor-trailer combinations. Eng. Appl. of Comput. Fluid Mech. 3, 587-607 https://doi.org/10.1080/19942060.2009.11015293
19. Mattetti M, Maraldi M, Lenzini N, Fiorati S, Sereni E, Molari G (2021): Outlining the mission profile of agricultural tractors through CAN-BUS data analytics. Comput. and Electron. in Agric. 184, 106078 https://doi.org/10.1016/j.compag.2021.106078
20. Mederle M, Urban A, Fischer H, Hufnagel U, Bernhardt H (2015): Optimization potential of a standard tractor in road transportation. landtechnik 70, 194-202 10.15150/lt.2015.2675
21. Morel T (1978): The effect of base slant on the flow pattern and drag of three-dimensional bodies with blunt ends, Aerodynamic drag mechanisms of bluff bodies and road vehicles. Springer, pp. 191-226
22. Mosiężny J, Ziegler B, Grzymisławski P, Ślefarski R (2020): Base drag reduction concept for commercial road vehicles. Energy 205, 118075 https://doi.org/10.1016/j.energy.2020.118075
23. Oh J, Choi K, Son G-h, Park Y-J, Kang Y-S, Kim Y-J (2020): Flow analysis inside tractor cabin for determining air conditioner vent location. Comput. and Electron. in Agric. 169, 105199 https://doi.org/10.1016/j.compag.2019.105199
24. Schäfer A, Heywood JB, Weiss MA (2006): Future fuel cell and internal combustion engine automobile technologies: A 25-year life cycle and fleet impact assessment. Energy 31, 2064-2087 https://doi.org/10.1016/j.energy.2005.09.011
25. Sivaraj G, Parammasivam K, Suganya G (2018): Reduction of aerodynamic drag force for reducing fuel consumption in road vehicle using basebleed. J. of Appl. Fluid Mech. 11, 1489-1495 10.29252/jafm.11.06.29115
26. Taghavifar H, Mardani A (2014): Analyses of energy dissipation of run-off-road wheeled vehicles utilizing controlled soil bin facility environment. Energy 66, 973-980 https://doi.org/10.1016/j.energy.2014.01.076

27. Templin J, Raimondo S (1986): Experimental evaluation of test section boundary interference effects in road vehicle tests in wind tunnels. J. of Wind Eng. and Ind. Aerodyn. 22, 129-148
28. Tian X, Cai Y, Sun X, Zhu Z, Xu Y (2019): An adaptive ECMS with driving style recognition for energy optimization of parallel hybrid electric buses. Energy 189, 116151 https://doi.org/10.1016/j.energy.2019.116151
29. Vignesh S, Gangad VS, Jishnu V, Krishna A, Mukkamala YS (2019): Windscreen angle and Hood inclination optimization for drag reduction in cars. Procedia Manuf. 30, 685-692 https://doi.org/10.1016/j.promfg.2019.02.062
30. Wiedemann J (1996): The influence of ground simulation and wheel rotation on aerodynamic drag optimization-potential for reducing fuel consumption. SAE Trans., 810-819
31. Xie S, Lang K, Qi S (2020): Aerodynamic-aware coordinated control of following speed and power distribution for hybrid electric trucks. Energy, 118496 https://doi.org/10.1016/j.energy.2020.118496
32. Xu F, Schillinger D, Kamensky D, Varduhn V, Wang C, Hsu M-C (2016): The tetrahedral finite cell method for fluids: Immersogeometric analysis of turbulent flow around complex geometries. Comput. & Fluids 141, 135-154 https://doi.org/10.1016/j.compfluid.2015.08.027

Figures

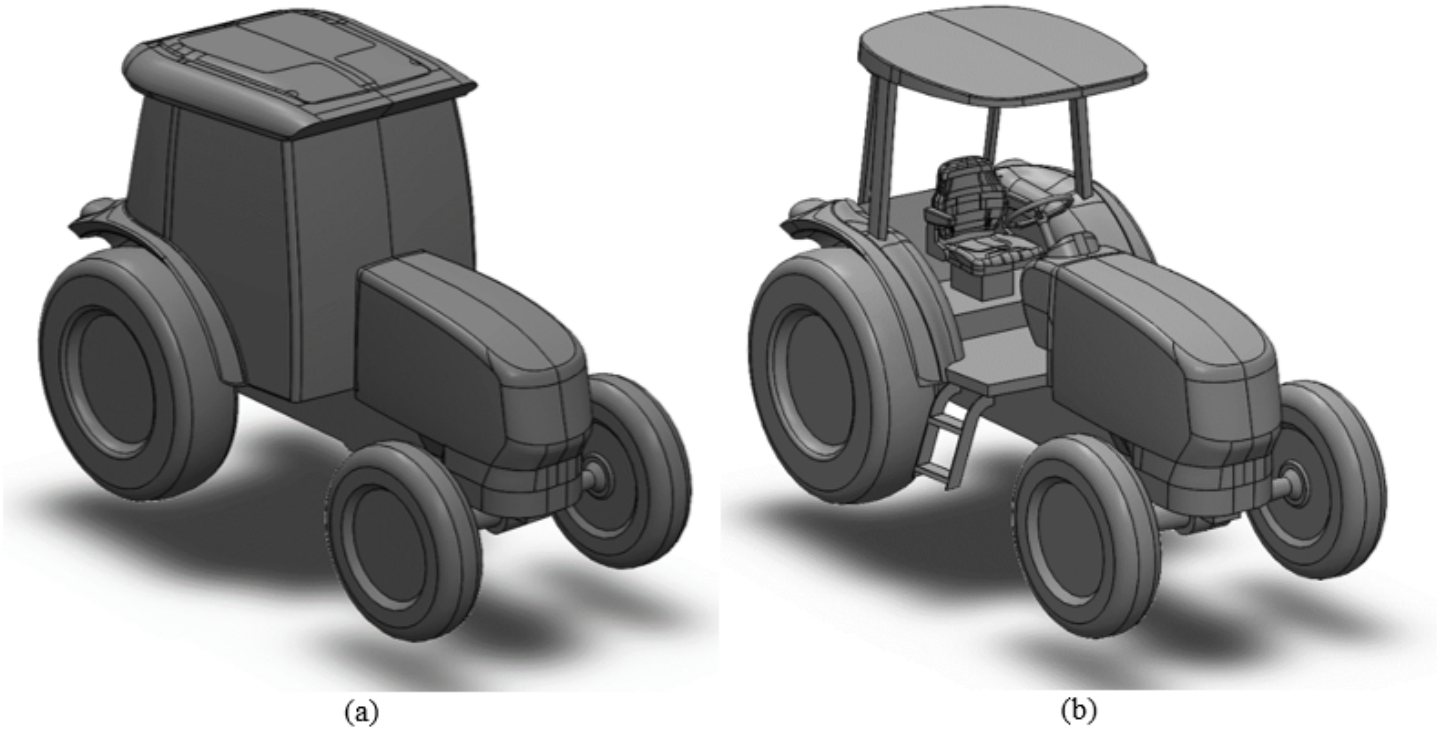

Figure 1

3D perspectives of the CFD models (a) cabin version (b) platform version

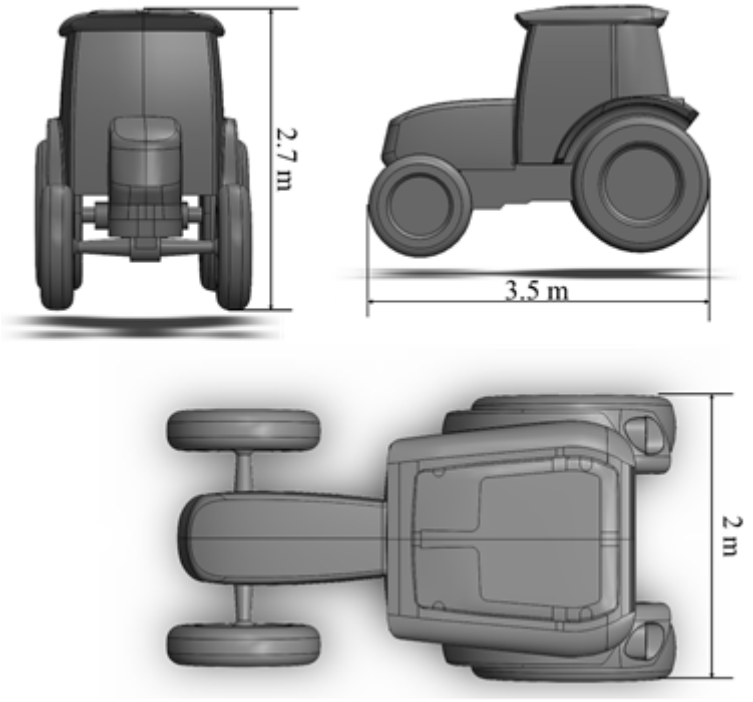

Figure 2

Dimensions of the 3D model

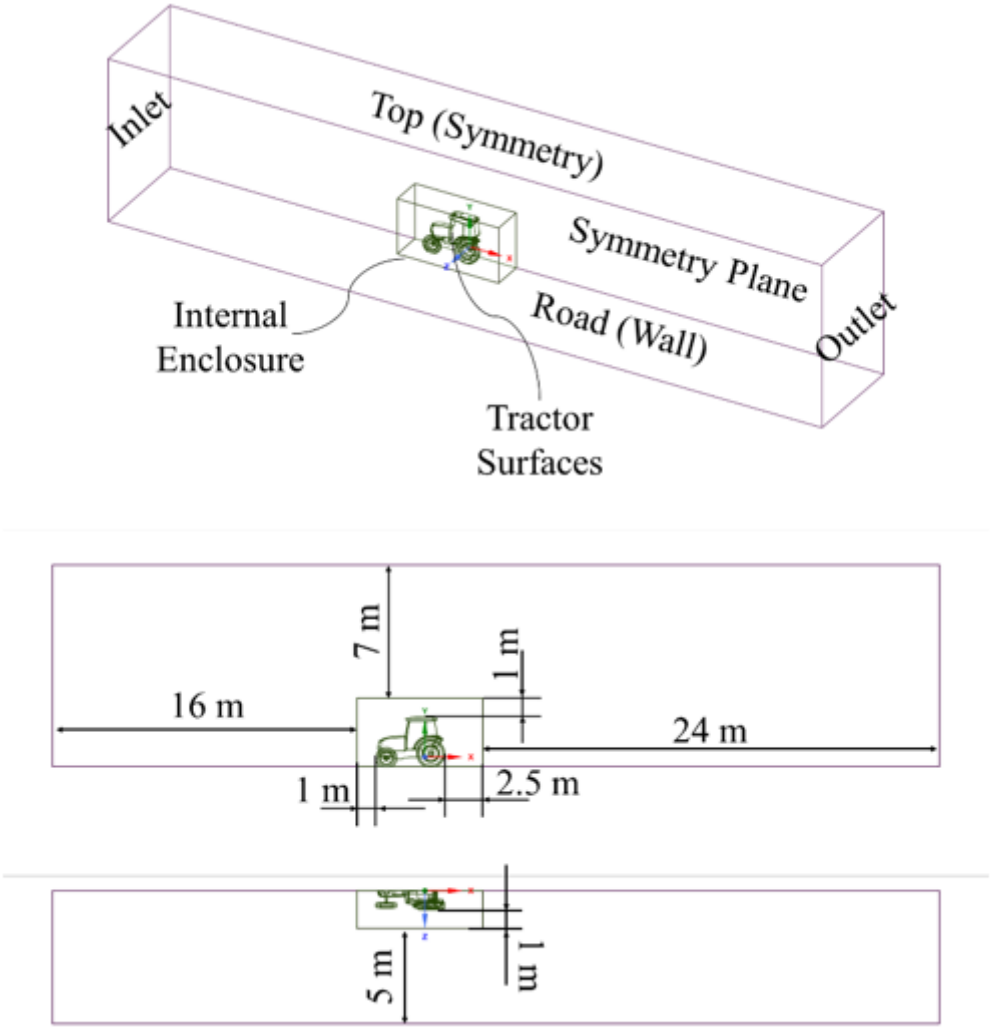

Figure 3

One side of symmetrical calculation domain; inner and outer enclosures; boundaries; dimensions

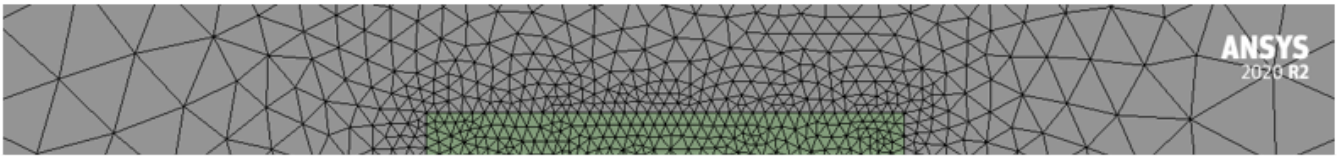

Figure 4

Mesh instances for cabin version of the tractor model (a) coarse (b) medium (c) fine

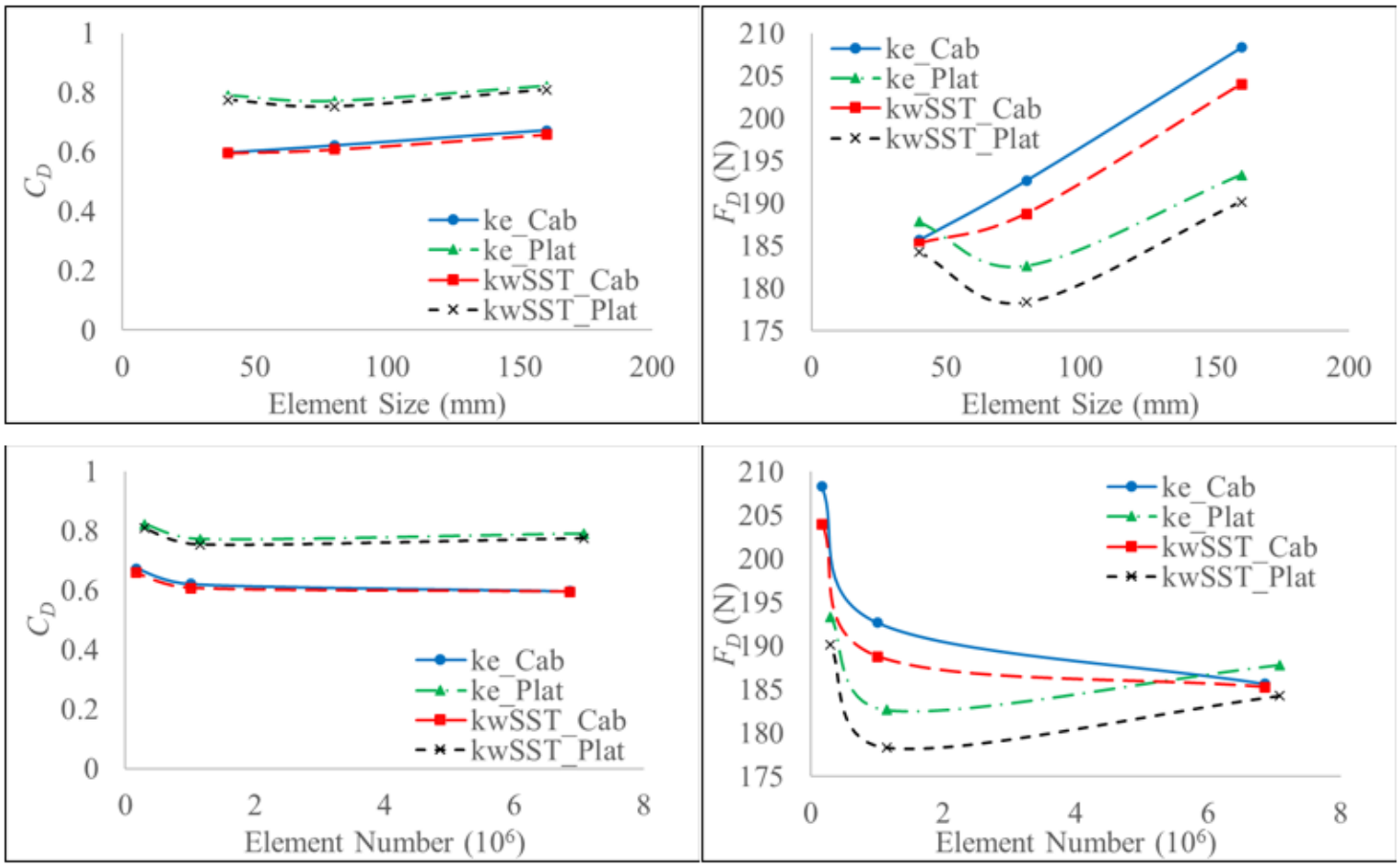

Figure 5

Changes in C_D and aerodynamic force acting on the tractor models according to internal enclosure element size and element numbers for 40 km/h travel speed

Figure 6

Evaluation of y^+ according to meshes for cabin version

Figure 7

Evaluation of y^+ according to meshes for platform version

Figure 8

Calculation domain by the characteristic length

Figure 9

Comparing turbulence models considering tractor wakes

Figure 10

Comparing turbulence models considering -10 Pa iso surfaces

Figure 11

Evaluation of y^+ according to meshes for cabin version

Figure 12

Evaluation of y^+ according to meshes for cabin version

Figure 13

Re independency of C_D values.

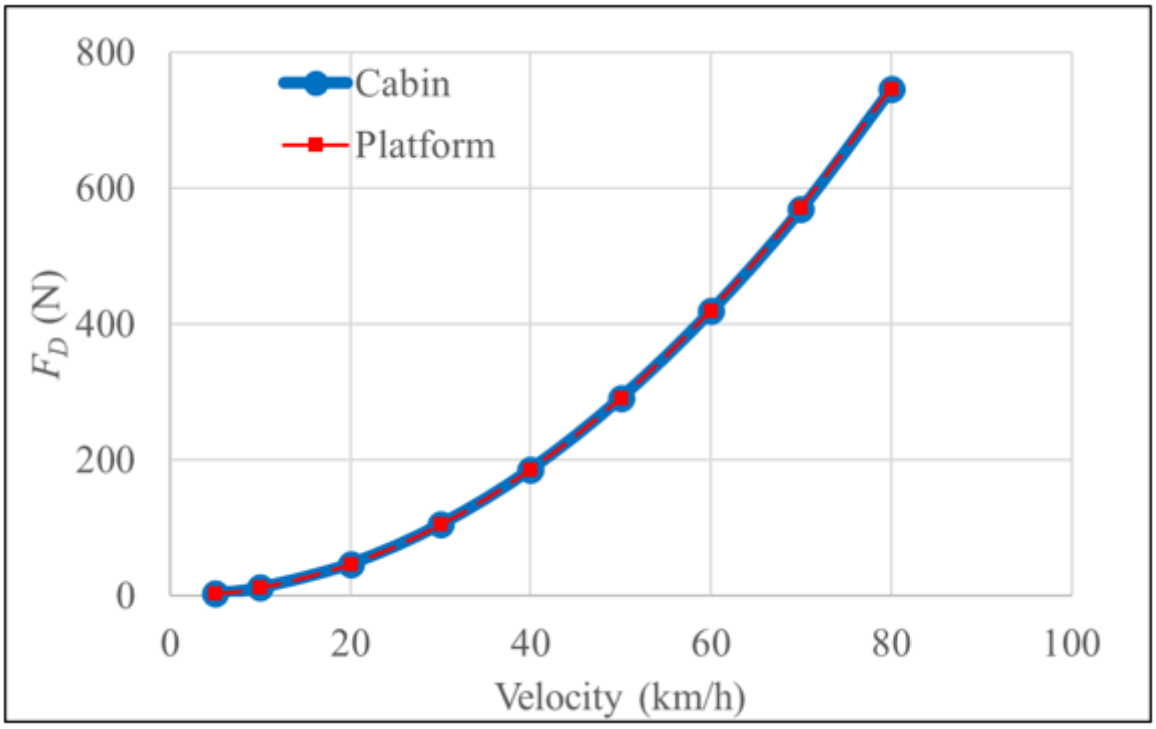

Figure 14

The proportionality between travel speeds and F_D.

Figure 15

Static pressure distribution on tractor surfaces

Figure 16

Velocity contours at the symmetry planes.

Figure 17

Turbulent kinetic energy contours at the symmetry planes.

Figure 18

Static pressure iso-surfaces downstream and proximity of the tractor models.

Figure 19

The power amounts that is necessary to overcome the aerodynamic resistance force.

Figure 20

The diesel fuel amounts that is necessary to overcome the aerodynamic resistance force.

Figure 21

The carbon emission amounts related to the aerodynamic resistance force.